X International Conference on Computational Methods in Marine Engineering
MARINE 2023
J. Garcia-Espinosa, L. González, J.E. Gutiérrez & B. Serván-Camas (Editors)

A Comprehensive Analysis of the Submarine Manoeuvring Forces at High Drift Angles

MARINE 2023

V.V. Zheku[*], D. Villa[2] and S. Gaggero[3]

[1] Department of Naval Architecture – DITEN, University of Genova, 16145 Genova, Italy

[2]Department of Naval Architecture – DITEN, University of Genova, 16145 Genova, Italy
Email: diego.villa@unige.it

[3]Department of Naval Architecture – DITEN, University of Genova, 16145 Genova, Italy
Email: stefano.gaggero@unige.it

[*] Corresponding author: Vito Vasilis Zheku, vitovasil.zheku@edu.unige.it

ABSTRACT

The use of underwater vehicles, not only for military but also for exploration, scientific and industrial purposes, is increasing, leading to higher demands on the designing of such vehicle types. For an underwater vehicle, the appropriate evaluation of its manoeuvrability characteristic is of crucial importance to guarantee its function within design parameters and safe operation. In a previous work carried out by the authors, the ability of numerical methods to reliably evaluate the manoeuvring forces experienced by the well-known DARPA-SUBOFF submarine was explored for a wide range of kinematic conditions. The same conditions explored by the experimental activities were simulated using an open-source RANS solver to calculate the hydrodynamic forces and moments. Unexpectedly, despite the results showing a good agreement with the experimental data for the fully appended configuration (the most relevant from a design point of view), for the barehull configuration the results show significant discrepancies. In the current study possible causes of these differences are investigated. The findings show that this issue arises from an underprediction of the effect of the shaded longitudinal vortexes in the suction side of the submarine. This discrepancy, even if it is quite small, affecting a large portion of the body, generates a not negligible error on the lateral force and its position. This consideration assesses the necessity for high-fidelity solvers to better predict these mall flow features to be able to correctly evaluate the maneuvering force of a slender body.

Keywords: DARPA-SUBOFF; RANS; kOmegaSSTLM; turbulence; manoeuvrability; underwater vehicles.

NOMENCLATURE

C_y	Sectional lateral force coefficient [-]
Y'	Lateral force coefficient [-]
N'	Yaw moment coefficient [-]
L	Length between the perpendiculars [m]
V	Free stream velocity [m s^{-1}]
ρ	Water density [kg m^{-3}]
y^+	Dimensionless wall distance
Re	Reynold's number [-]
CFD	Computational Fluid Dynamics
URANS	Unsteady Reynolds-Averaged Navier-Stokes
AUV	Autonomous Underwater Vehicles

LES Large Eddy Simulation
DES Detached Eddy Simulation

1. INTRODUCTION

The study of submarine maoeuvrability has long been an area of interest in naval research. It is a critical aspect of underwater operations, allowing submarines to navigate through complex and challenging environments with precision and safety. The ability of a submarine to manoeuvre efficiently and effectively is influenced by various factors, including its shape, propulsion system, control system, and, as expected, the experience and skill of its helmsman.

In the past, experimental data were the only available way to gain insight into the hydrodynamic forces and moments that occur during submarine manoeuvres. However, the cost and complexity of such experiments make them often prohibitive for routine use. In recent years, computational fluid dynamics (CFD) has become an increasingly important tool for analysing and optimizing the hydrodynamic performance of vessels (such as in Franceschi *et al.*,2021 and Piaggio *et al.*, 2020) or submarines. CFD simulations involve the use of mathematical models and numerical algorithms to solve the governing equations of fluid motion, allowing researchers to predict and visualize the flow patterns around a submarine and assess its hydrodynamic performance. This procedure is helpful, especially in an early design phase, in order to suggest design modifications that can improve the overall manoeuvrability of the submarine. As a consequence of that, the costs for these types of evaluation (both CFD based and experimentally based) should be as little as possible.

Several studies have demonstrated the utility of CFD simulations in analysing and optimizing submarine manoeuvrability. For example, Dubbioso *et al*. (2017), using numerical simulations carried out with an in-house developed CFD solver, evaluated the impact of the stern appendages configuration on the turning characteristics of a fully appended national submarine (analysing the submarine model named CNR-INSEAN 2475). The authors examined the cross and X rudder configurations under two main operating scenarios: snorkelling depth and open water. In a similar way, Broglia *et al*. (2020) examined the "BB2" submarine vortices shed during pitch advancement and steady drift under four operative conditions: straight ahead, constant drift angle, and for both positive and negative pitch angle. The calculations showed that the negative pitch manoeuvre had the biggest effect on the sail vortices on the submarine aft part, affecting both the stern appendages and the propeller plane. In a study by Zhang *et al*. (2018), the unsteady Reynolds-Averaged Navier Stokes (URANS) method was used to simulate the surfacing motion of a submarine model (submarine named DARPA-SUBOFF) in regular waves. Their results showed that the underwater roll and pitch instability occur in the proximity of the free surface.

Among the several CFD methods that have been used in literatue, the Reynolds Average Navier-Stokes (RANS) method is the commonly used method for simulating the steady-state flow around submerged bodies, thanks to their low-computational requirements, but when complex instabilities are of interests, the more advanced CFD method Large Eddy Simulation (LES) can capture unsteady flow phenomena with higher accuracy. A relevant study has been published by Fureby *et al*. (2016) which includes the analyses of the flow features generated by a submarine under straight-ahead and sideslip conditions, getting good agreement between the outcomes of the simulation and the Particle Velocimeter Image (PIV) measurement. Posa and Balaras (2016), by using the high-fidelity LES method, published the results of a computational study on the flow around a submarine model, examining how the appendages affected the propeller wake fields. In studying the formation of the boundary layers at various sites, Morse and Mahesh (2021) offered their fresh contribution to the analysis of turbulent boundary layers on streamlined bodies. Using large eddy

simulation and a wall-layer model, Rocca *et al*. (2022) carried out a numerical characterization of the hydrodynamic and hydroacoustic field of a hypothetical underwater vehicle geometry. Nonetheless, the LES method requires significantly more computational resources than the RANS method, which limits its application to large-scale simulations. In recent years, Detached Eddy Simulation (DES) has emerged as a promising method for predicting the flow around a submarine. Combining the RANS and LES methods, DES can capture both the steady and unsteady flow phenomena around submerged bodies. The DES method, employing RANS method for the attached boundary layer and LES method for the separated flow regime, can provide accurate predictions of the hydrodynamic coefficients while maintaining a reasonable computational cost. Due to the benefits of the DES method several studies have been performed utilizing this approach. A complete examination of the flow around a submarine model under straight-ahead and static drift conditions was reported by Lungu (2019,2022), who used a variety of turbulence models to evaluate the specific problems of large-scale flow separation involved. In a series of numerical experiments for submarine geometries operating close to the free surface, Wang *et al*. (2019, 2020) found that the existence of the hull and the interaction with the free surface had a significant impact on the propeller performance. A numerical study of vertical zigzag manoeuvre for a submarine model was also presented by Carrica *et al*. (2021). The authors discussed the importance of scale effect on the hydrodynamic forces and manoeuvring motions. In Liu *et al*. (2021b) investigation of the flow fields around a submarine model under conditions of high Reynlods numbers, they examined the ability of the numerical approach to forecast the impacts of surface curvature on the turbulent boundary layers. Haipeng *et al*. (2023) performed a numerical study for the flow around the submarine under the rudder deflection condition, comparing the results obtained by URANS and DDES. In tight manoeuvring conditions with notable flow separation, the DDES approach offered a better capability for recording the flow field characteristics around the submarine.

While CFD has shown promise in predicting the hydrodynamic performances of submarines, it is important to validate the accuracy of CFD predictions against experimental data. Several researchers have conducted experiments to measure the hydrodynamic forces and moments on manoeuvring submarines. Kumar *et al.* (2012) conducted Particle Image Velocimetry (PIV) measurements on the Defence Science and Technology Organisation (DSTO) generic submarine geometry at different side slip angles. Manshadi *et al.* (2017), conducted both experimentally and numerically the effect of using the vortex generators on the flow field characteristics of the SUBOFF submarine model. The tests consisted of oil flow visualization carried out in an open loop low subsonic wind tunnel with three different sizes of vortex generators. The results showed that the hydrodynamic performance is superior to the barehull model when mid-vortex generators are utilized, lowering both the cross-flow separation and the drag force. Efremov *et al.* (2019) conducted an experimental program of towing and PMM captive tests of DARPA SUBOFF for the case of close free water surface operation. Khan *et al.* (2022) carried out surface pressure measurements on a generic submarine hull form (SUBOFF), by a series of model tests in Wind Tunnel Facility at Naval Science & Technology Laboratory, India. It is obvious how one notable campaign of experiments is the DARPA-SUBOFF case conducted at the David Taylor Research Centre (DTRC) (Roddy, 1990), which provides valuable data for researchers to compare their CFD predictions and improve the accuracy of the simulations.

In a previous work carried out by authors (Zheku *et al.*, 2023) the ability of numerical methods to reliably evaluate the manoeuvring forces experienced by the DARPA-SUBOFF was explored for a wide range of kinematic conditions. The experiments were simulated using an open-source RANS solver to calculate the hydrodynamic forces and moments. Unexpectedly, despite the results showing a good agreement with the experimental data for the fully appended configuration (the most relevant from a design point of view), for the barehull configuration the results show significant discrepancies at high drift angles. Being the hull of the DARPA-SUBOFF, a simple solid of revolution, it can be considered a valuable geometry, very similar to the ones often used for small-size autonomous underwater vehicles (AUV). The importance of a detailed understanding of the flow around a submersible hull is straightforward to investigate the force experienced by the body reliably. Previous studies have suggested the presence of cross-flow separation around such shapes (seen as two big longitudinal vortices), which might be the main reason for the discrepancies (among the other: Kotapati-Apparao *et al*., 2003; Subrahmanya *et al*., 2019; Chesnakas *et al*., 1997). Similarly, previous CFD calculations show this flow feature given by two intense counter-rotating vortices, even if the measured and predicted forces did not agree well.

In order to better capture these vortices, and accurately analyse the manoeuvring performance of these simple shapes that generate complex flow field in strong off-design conditions, in the current paper some preliminary analyses have been performed to assess the main possible numerical causes for the previously highlight differences. The paper is organized initially describing the computational set-up in section 2 and the considered test case in section 3. Section 4 is devoted to describing the previous finding where the aim of the present paper was born. Then in the result section (number 5) a detailed description of all the findings is reported. Finally, the main conclusions are summarized in the last section.

2. METHODOLOGY AND COMPUTATIONAL SETUP

In the current paper, numerical simulations are performed with the open-source CFD library OpenFOAM. Considering the overall computation aspects, in particular in light of the design requirements to keep the computational burden as low as possible, a steady-state solver is used. Second order schemes have been considered to keep high the accuracy of the solver, but, for some quantities, some relaxation factors have been considered to guarantee a stable solution. The solver is mainly based on the consistent version of the the SIMPLE (Semi-Implicit Method for Pressure-Linked Equations) algorithm, which is properly designed to solve an incompressible steady state problem (Van Doormaal and Raithby, 1984). The overall domain is meshed by the OpenFOAM native grid generator using a procedure already described in previous papers (see among the other Franceschi *et al.*, 2021). It generates a uniform cartesian mesh further refined in the near-field regions and in the wake field, and then adapted onto the real boundary shape to obtain a body-fitted shape. The computational domain around the submarine model is a prismatic box with the upstream boundary at $2L$ ahead of the fore part of the submarine, where L is the length of the underwater vehicle, the downstream boundary at $3L$ from the stern, and lateral sides, as well as the bottom boundaries at $1.5L$ from the cylindrical body (Fig. 1). The assigned boundary conditions are also shown in Fig. 1.

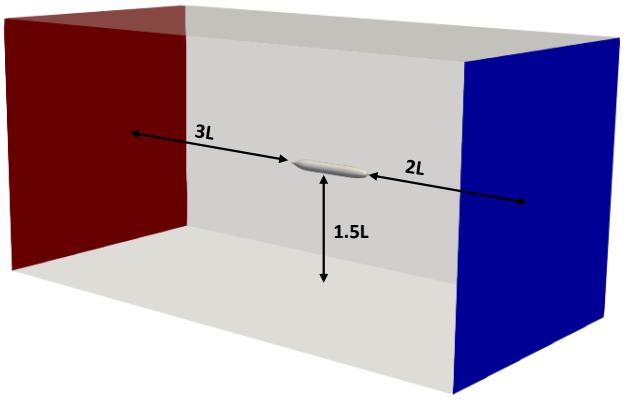

Figure 1. Main dimensions of the computational domain.

A velocity inlet is assigned to the right side of the computational domain (shown in blue in the figure), and a pressure outlet is forced on the left (in red). While the submarine surfaces are given a no-slip wall condition, the other surfaces are taken into consideration as symmetry planes to represent the far-field condition. The domain sizes are such that the far-field flow can be considered undisturbed, preventing the boundary conditions from having an impact on the flow field around the submarine and its associated forces. More details on the selected dimensions can be found in Roddy (1990). As already reported, the present paper analyses the possible issues connected with the previously mentioned discrepancies between CFD and experimental measurements. Among all the considered sources of uncertainty, the influence of the adopted turbulence models is considered. Therefore, different turbulent models have been taken into account and their impact on the force has been investigated. A limited number of conditions, where crossflow and then, the differences currently observed with experiments are more pronounced (i.e., high drift angles), will be considered.

3. TEST CASE

The underwater vehicle under investigation is the well-known SUBOFF model, designed and tested in the David Taylor Research Centre (DTRC) for the Defense Advanced Research Projects Agency (DARPA). While the equations required to create the model geometry can be found in the reference literature (Groves *et al.*, 1989), Fig. 2 provides the model primary dimensions and its reference system. The hull symmetry axis, which is located at $x = 2.013m$ with respect to the aft perpendicular (see Fig. 2) and corresponds to the mid-point between the perpendiculars, is where the chosen reference frame is centred.

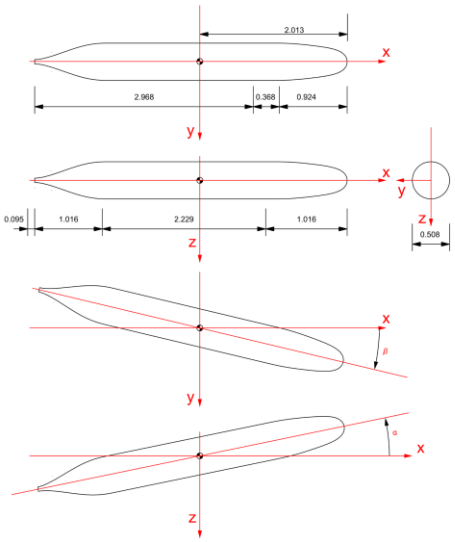

Fig 2. Reference system and DRAP SUBOFF main dimensions.

The x-axis is positive pointing towards the fore part of the submarine, the y-axis pointing towards the starboard side and the z-axis pointing downwards. The submarine rotates positively towards the starboard side. All the forces and moments will be referred to in the ship reference frame (fixed with the ship itself).

4. PREVIOUS RESULTS

As mentioned in the introduction, in the author's previous work, an extensive validation of RANS methodologies was presented, on the DARPA-SUBOFF, at four different configurations. The study aimed at consolidating the reliability of the CFD simulations to predict the hull and the appendages forces during a manoeuvre of underwater vehicles to be adopted to feed a mathematical model devoted to predicting the real manoeuvring behavior of a generic submarine or underwater vehicle. The mesh independence analysis was verified using three different meshes, and the finding revealed a converging trend of the global forces with a relatively low-demanding mesh arrangement of 3M cells, which represents a good trade-off between the computational time and the accuracy of the results. The expected numerical uncertainty on the primary manoeuvring forces was within 2%. The linear part was captured in an excellent way (see Fig. 3), whereas two streamwise vortices were noticed to have a crucial impact on the non-linearities present in the bare hull configuration in the drifting attitudes. Fig. 3 shows the comparison between the simulated data and those obtained by the experiments of the DTRC.

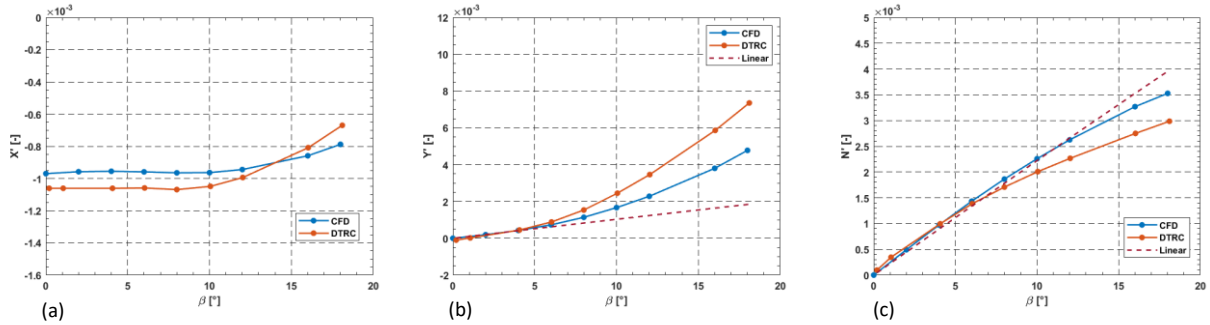

Figure 3. Comparison between the numerical results (blue) and the experimental data (orange) of $\boldsymbol{X'}$, $\boldsymbol{Y'}$ and $\boldsymbol{N'}$ for the barehull configuration. The linear component showed in dashed line.

Nonlinear phenomena become more noticeable for drift angles greater than 6°, resulting in a significant discrepancy between the data obtained from the numerical simulations (orange) and the measured data from the experimental tests (blue). The author stated that a possible cause of this discrepancy might be the cross-

flow separation. Fig. 4 makes clear how changing the drift angle affects the surface pressure distribution and the cross-flow in the boundary layer. This occurrence causes two symmetrical streamwise vortices to form, which originate from the downstream side of the body. These vortices become more prominent and extensive as the drift angle increases (Kim *et al.* 2013). Similar effects have been generally observed also by previous numerical investigations on the flow around a prolate spheroid, similar to the geometry of the current hull (Hoang *et al.*, 1994; Kotapati-Apparao *et al.*, 2003; Subrahmanya *et al.*, 2019; Chesnakas *et al.*, 1997).

Figure 4. Surface pressure contours and limiting wall streamlines on the barehull for three different drift angles $\boldsymbol{\beta}$=4° (lower), 10° and 18° (upper).

The results of Kotapati *et al.* (2009) and Subrahmanya *et al.* (2019) are replicated when the vortices region is examined in more detail (Fig. 5). The vortices in Fig. 5(a)-(c) have flat elliptic shapes and are located near to the hull for modest drift angles. The vortex begins to separate from the body, becomes larger and takes on a more circular shape as the section gets closer to the stern and the drift angle increases (Fig. 5(g)-(i)).

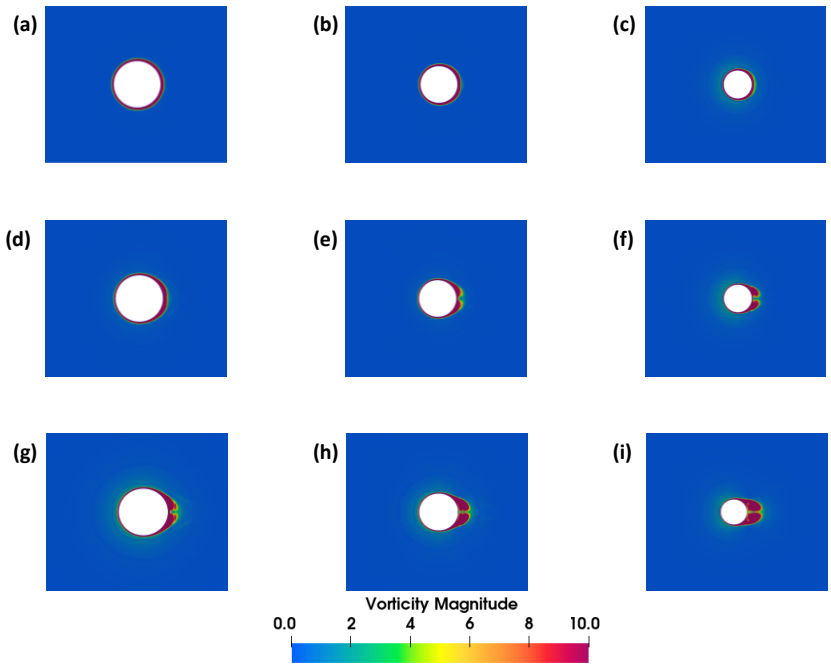

Figure 5. Vorticity around the axisymmetric hull for 4° (a)-(c), 10° (d)-(f) and 18° (g)-(i) of drift angles, sections at 0.55$\boldsymbol{L}$, 0.35$\boldsymbol{L}$ and 0.15$\boldsymbol{L}$.

Fig. 6, showing the sectional forces, provides another important clue that aids in determining where the mistake of the estimates lies. The submarine has been divided into 100 transversal sections and the forces acting on each section were measured. The sectional lateral force coefficient C_y values acting on the bare hull configuration are represented by the blue line. This coefficient is calculated as shown below:

$$\frac{100 \times Y_{\text{sectional}}}{\frac{1}{2}\rho V^2 L^2} \tag{1}$$

Where $Y_{sectional}$ is the force acting of the 100 sections that the hull was divided, ρ is the water density, V the model scale velocity of experiments, equal to 3.34 m/s and L the distance between the perpendiculars.

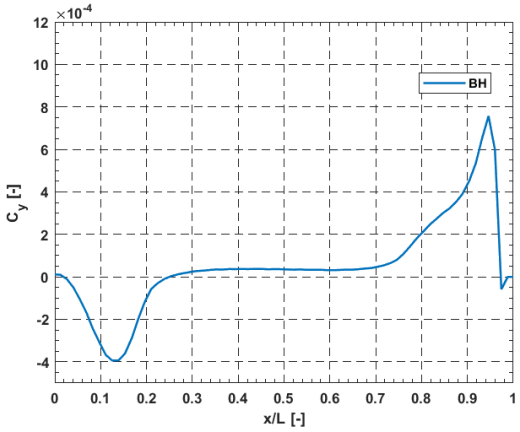

Figure 6. Predicted sectional lateral force coefficient for the BH (barehull) configuration.

A suggestion that the forces and moments there predicted may be the cause of the differences in this configuration can be observed in the fact that the vortices, previously stated, have the greatest influence on the pressure fields towards the stern of the hull. Given that the recorded lateral force acting on the barehull was underestimated, the authors tried a potential alternative distribution of the sectional forces at the stern area, where the peak of the negative values is present. Their finding demonstrates that a correction of the stern forces generates a contemporary better agreement on the later force and yaw moment with respect to the measurements, demonstrating that this is the region where a problem must be searched.

5. RESULTS: INFLUENCE OF ADOPTED TURBULENCE MODELS

5.1 Mesh Analysis

To address the aforementioned differences many attempts in this regard were undertaken in the current research and contrasted both with the experimental results and among them. As a finer mesh offers better spatial resolution and captures more information about the flow field, including turbulence, flow separation, and small-scale vortices, in which the current study is interested in, a first approach was that of increasing the number of the cells. Fig. 7 shows the used meshes, $grid\ I$ is the coarsest mesh (2M cells), $grid\ II$ (3M cells), $grid\ III$ (7M cells) and the finest $grid\ IV$ (11M cells).

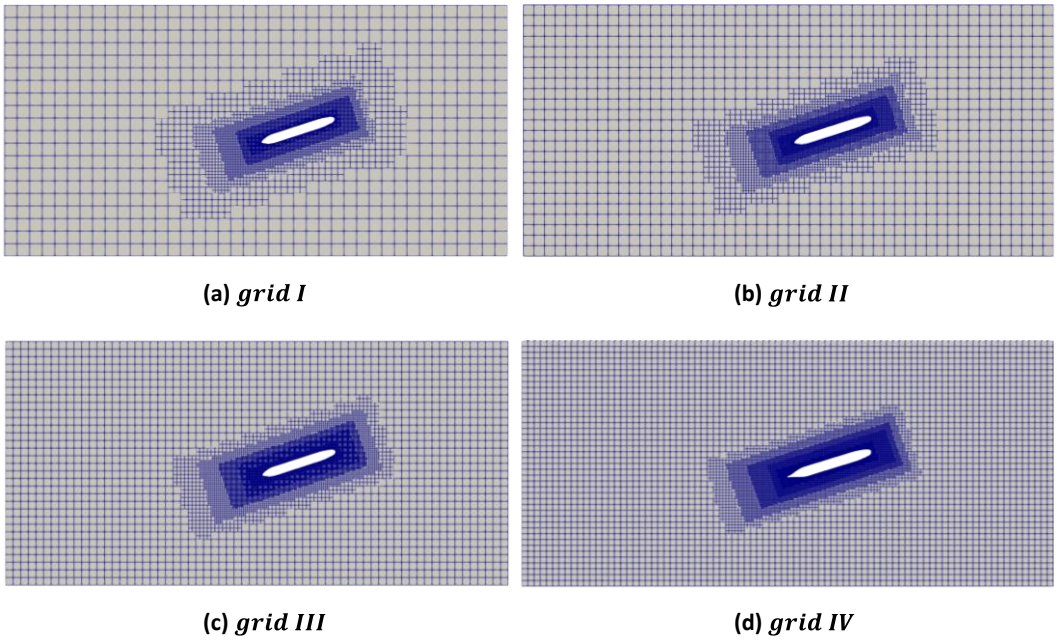

Figure 7. The four different mesh grids; (a) 2M, (b) 3M, (c)7M and (d) 11M.

Tab. 1 shows the results for the non-dimensional lateral force Y' and yaw moment N' obtained from the simulations with the four different grids for the 4°, 6° and 18° drift angles. These angles have been considered to simultaneously verify how the results change in a linear range (for the lowest value), when some uncertainties arrases (intermediate angle) and when the issue occurs at very high angles (for the highest considered also experimentally).

Table 1. Comparison between the experimental data and the results of the four different grid meshes for three different drift angles (4°, 6° and 18°)

	DTRC	***Grid I***	***Grid II***	***Grid III***	***Grid IV***
$\boldsymbol{Y'_{4^\circ} \times 10^{-4}}$	4.49	4.22	4.27	4.31	4.49
$\boldsymbol{N'_{4^\circ} \times 10^{-4}}$	9.96	9.56	9.67	9.73	9.80
$\boldsymbol{Y'_{6^\circ} \times 10^{-4}}$	8.86	7.22	7.29	7.47	7.79
$\boldsymbol{N'_{6^\circ} \times 10^{-3}}$	1.385	1.444	1.433	1.422	1.408
$\boldsymbol{Y'_{18^\circ} \times 10^{-3}}$	7.355	4.844	4.778	4.875	5.204
$\boldsymbol{N'_{18^\circ} \times 10^{-3}}$	2.986	3.506	3.526	3.526	3.482

Fig. 8 shows the trend of the non-dimensional lateral forces (a) and yaw moment (b) acting on the body (black line) calculated with *grid IV*, compared to the experimental data and the predicted values with *grid III*. The simulations concerned three drift angles, 4°, 6° and 18°. It is clear how the linear part is always

well predicted as in the previous work, whereas for high drift angles, even though an improvement can be noticed, still the lateral forces are under predicted, whereas the values of the yaw moment are almost the same as those calculated with *grid II*. These results demonstrate that, even if a very demanding mesh is used, no improvements are noticed in the results. This assesses that the issues cannot be related with the mesh description or the numerical solution of the considered mathematical problem.

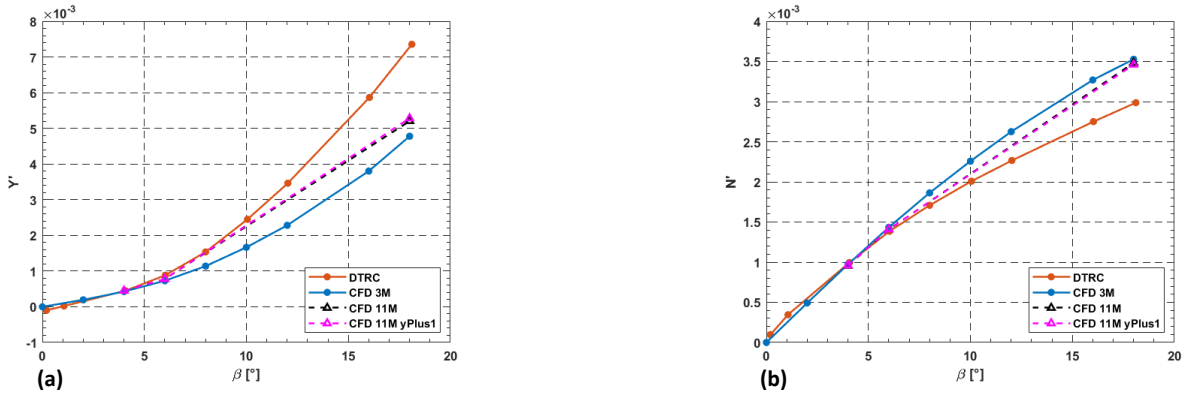

Figure 8. Comparison between the experimental data and the results of the 3M cells mesh, the 11M cells mesh and the 11M cells mesh having $\boldsymbol{y^+}$lower than 1.

Another possible drawback is the solution of the boundary layer. The mean values of y^+ of the previous simulations are between 30 and 50, a good compromise between accuracy and computational cost of the simulation (Pope, 2000). Additionally, this range of y^+ values, perform well with some turbulence models such as the k-omega SST model (Menter, 1994), used in the previous in these simulations. Nonetheless, using a y^+ value less than 1 is recommended for accurate modeling of the near-wall region, as the first computational cell is located within the viscous sublayer, region where the viscous forces are dominant. For this reason, another attempt in order to better model the near-wall region and predict the flow properties a mean y^+ lower than 1 was achieved. Fig. 9 illustrates the y^+ values on the submarine hull in the case of y^+ lower than 50 (left) and that lower than 1 (right). In Fig. 10, the two different obtained boundary layers are shown at the fore part of the hull. It is quite clear how the boundary layer of the submarine with lower y^+ has more layers.

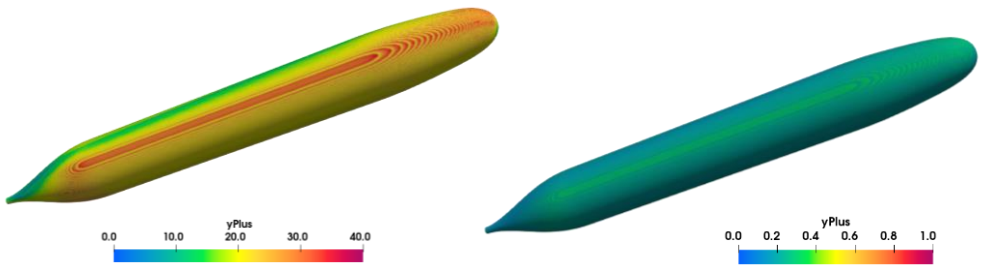

Figure 9. The values of the yplus over the barehull for the two cases: 30 < $\boldsymbol{y^+}$< 50 (left); $\boldsymbol{y^+ < 1}$ (right).

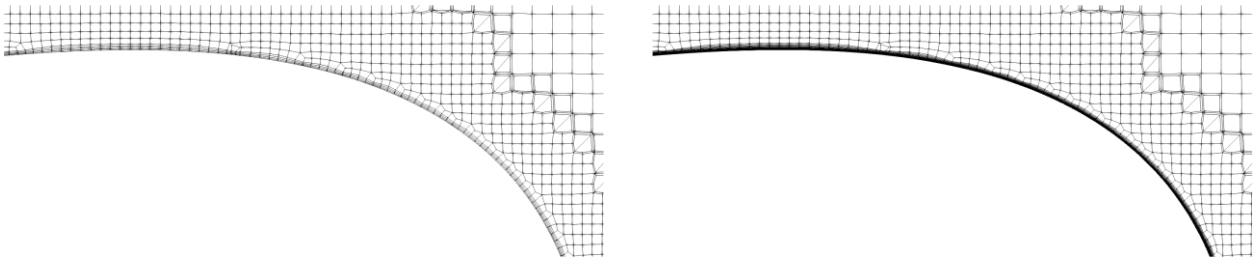

Figure 10. Boundary layer of the aft part of the DARPA SUBOFF for $\boldsymbol{y^+}$ lower than 1 and $\boldsymbol{y^+}$ lower than 50.

In Fig. 8 in magenta colour the trend of this calculation is also presented. Comparing the obtained values with $grid\ I$, having y^+ lower than 1 ($Y' = 5.20 \times 10^{-3}; N' = 3.48 \times 10^{-3}$) and y^+ between 30 and 50 ($Y' = 5.28 \times 10^{-3}; N' = 3.46 \times 10^{-3}$), it is evident that the discrepancy between the two is negligible for both the lateral force and the yaw moment. Still as before the lateral forces are underestimated, thus it is straightforward how for this specific application and turbulence model (k-omega SST) the benefits of using a y^+ value less than 1 may not be significant enough to justify the increased computational costs.

5.2 Turbulence Models

As noted earlier, a possible explanation of the discrepancies between the predicted Y' and N' and the measured ones might be the generation of the two symmetric streamwise vortices. From this point of view, the choice of the used turbulent model is important (see Wackers *et al.*, 2015). Thus, four different turbulence models present in the open-source software OpenFOAM are tested. In the following paragraphs a comparison between these models (*kOmegaSST, kOmega, kEpsilon, realizablekEpsilon)* is presented. Fig. 11 shows the comparison between vorticity around the axisymmetric hull modelled with kOmegaSST (a), kOmega (b), kEpsilon (c) and realizablekEpsilon (d). It is evident how the two first turbulence models describe in a similar way the shaded vortices. However, small differences are present such as the vorticity magnitude in the centre of the vortices, regions with higher values (yellow and red scale) become slightly larger. The vortices become larger and more distant both from the body and between each other. Differently, the kEpsilon models appear more intricate and detailed, with more small-scale structures and irregularities, whereas the kOmega models appear smoother and simpler.

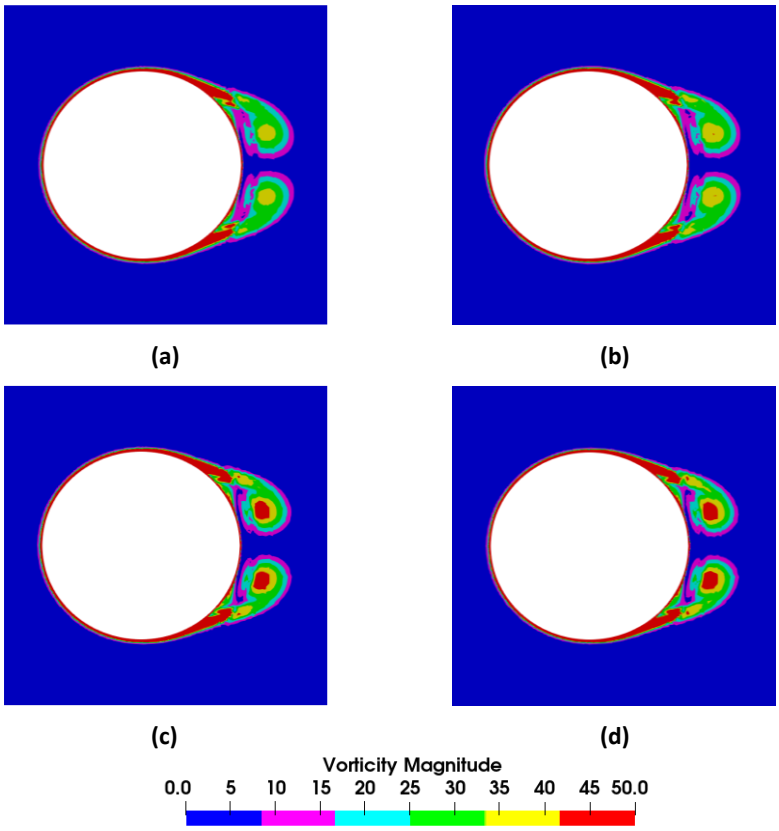

Figure 11. Vorticity around the axisymmetric hull modelled with kOmegaSST (a), kOmega (b), kEpsilon (c) and realizablekEpsilon (d).

Fig. 12 shows both the values of the pressure coefficient as well as the wall shear stress over the hull. The negative pressure created by the two vortices is more evident with kEpsilon based models. Also, more detailed values of the wall shear stress can be noticed in these models. The pressure distribution at the fore part of the submarine hull is substantially the same for all the turbulence models used, the differences start where the vortices are present. On the other hand, small differences can be noted in the region where the wall shear stress is higher in the aft part. These differences might lead to the different predicted lateral forces and yaw moments. Tab. 2 shows the comparison between the experimental data and the predicted values with the different turbulence models for 18° drift angles.

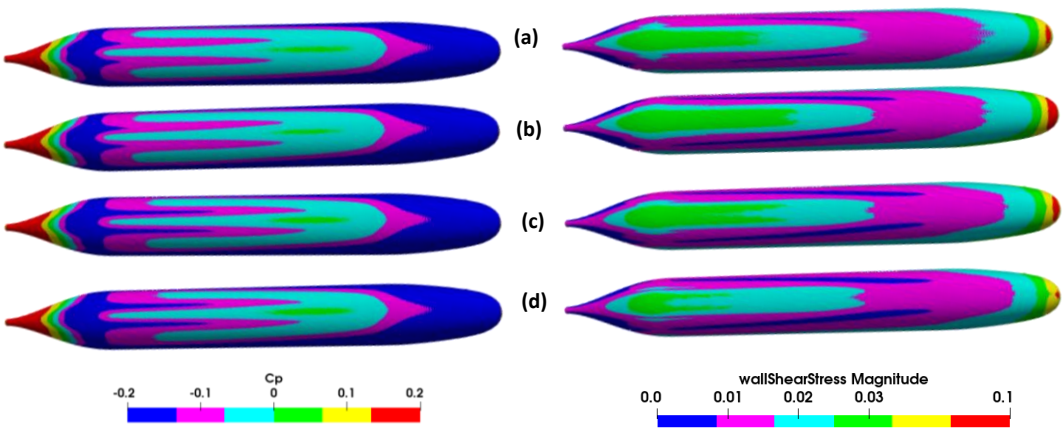

Figure 12. Pressure coefficient and wall shear stress magnitude over the submarine hull for the four different turbulence models: kOmegaSST (a), kOmega (b), kEpsilon (c) and realizablekEpsilon (d).

Another interesting aspect regards the previously mentioned sectional forces. Fig. 13 shows the sectional forces acting on the hull for the different turbulence models used in the simulations. It is clear how the closer to the experimental results the calculations are, the less the negative force in the stern region. Fact that validates the initial hypothesis of the authors, that the magnitude of the force at the stern is overestimated by the initial simulations. These results can also give a hint on the effect that small differences in the pressure field can generate significant variations in the later force intensity and position. This is mainly due to the fact that during the manouvre the later force is caused by the difference between the positive bow force and the negative stern part. As a consequence of that, if a small discrepancy is located locally on the pressure field it has an important effect on the overall force.

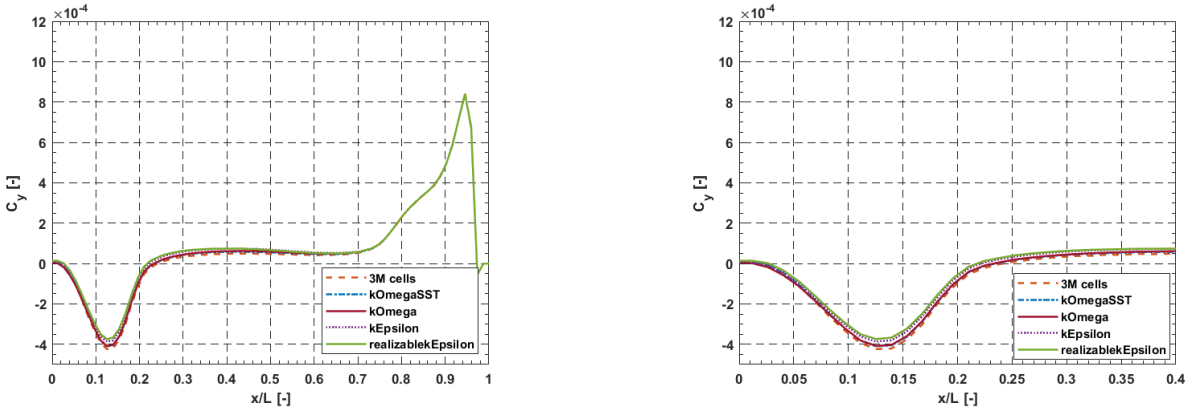

Figure 13. Comparison between the sectional forces of the simulations with the different turbulence models; A closer look to the region where the main differences are present.

In order to better understand where the problem of the differences between the experimental data and the simulated ones, a closer look to the pressure field and the values of wall shear stress around the various sections of the hull is important. Fig. 15 illustrates the pressure field and the wall shear stress around two different sections of the barehull (see Fig. 14) with 18° drift angle. The comparison is limited to kOmegaSST and realizablekEpsilon turbulence models because they show the main differences.

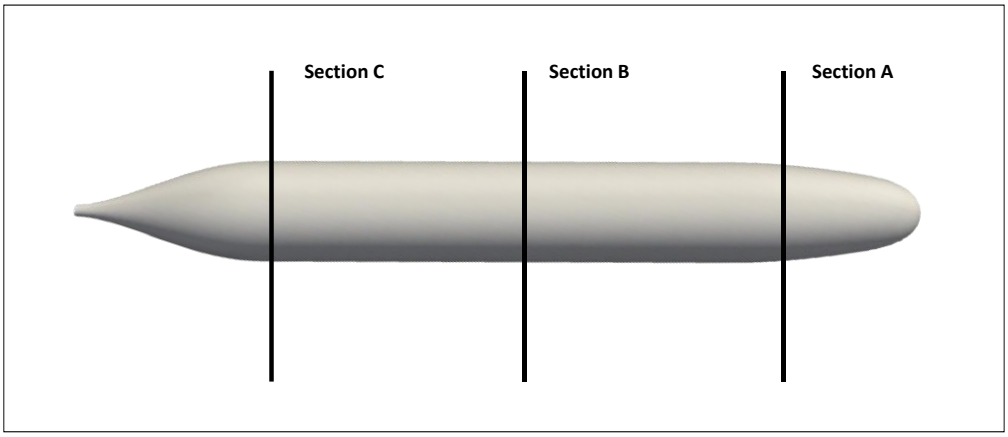

Figure 14. Sections where the pressure distribution and the wall shear stresses are illustrated; Section A located 3.5 m from the aft perpendicular, section B, 1.5 m and C, 0.6 m.

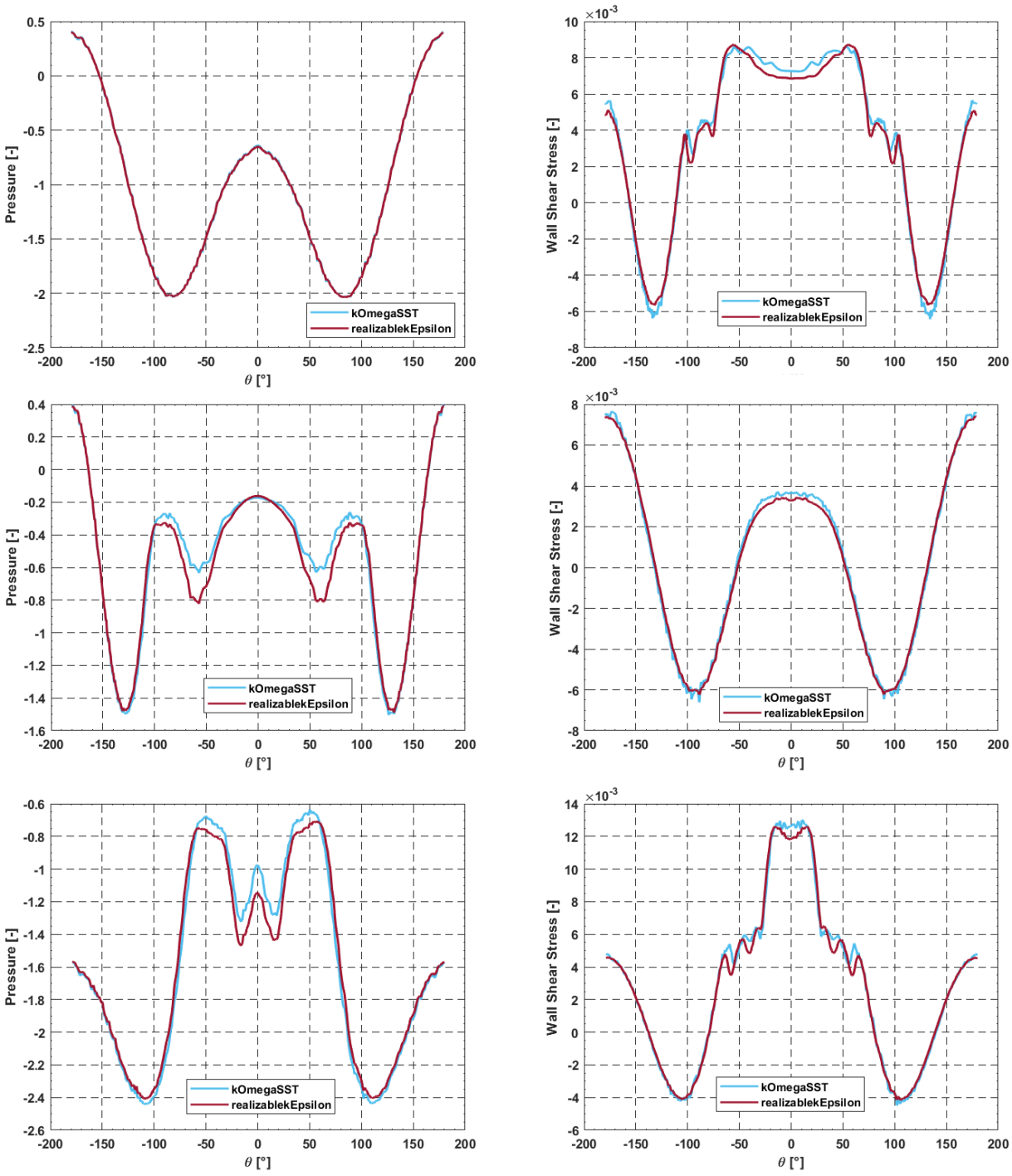

Figure 15. Pressure distribution and values of the lateral component of wall shear stress around the hull in three different sections (A, B and C); the values obtained from the kOmegaSST and realizablekEpsilon are compared.

The top graphs show the pressure distribution and the wall shear stress values in section A, located at 3.5 m (corresponding to x/L=0.8) from the aft perpendicular. As the vortices have a small influence in that region of the hull, it is straightforward how the two different turbulence models give almost the same outcomes, especially for the pressure distribution, whereas small differences are present in the y-component of the wall shear stress. Looking at Fig. 13, at that section, as expected, no differences between the two lateral sectional forces can be noticed. On the other hand, the mid and bottom graphs show the same quantities at section B, located at 1.5 m (corresponding to x/L=0.3) from the aft perpendicular and at section C, located at 0.6 m (corresponding to x/L=0.14) from the aft perpendicular. Significant differences between the two models

concern the pressure distribution can be seen. These differences are concentrated in a small part of the peaks of depression but still the differences in the lateral sectional forces (Fig. 13) are visible. The above consideration might give a hint on the small influence of the wall shear stress component in the lateral force and the greater influence that the pressure field might have.

Table 2. Comparison of the values of lateral force and yaw moment between the experimental data and the and the outcome of the kOmega and kEpsilon turbulence models.

	DTRC	***kOmegaSST***	***kOmega***	***kEpsilon***	***realizablekEpsilon***
$Y'_{18^\circ} \times 10^{-3}$	7.355	5.204	5.364	5.966	6.139
$N'_{18^\circ} \times 10^{-3}$	2.986	3.482	3.477	3.346	3.264

Fig. 16 illustrates the comparison between the values of the Tab 2, also for the 4° and 6° drift angle. As before being the linear part well predicted, the several turbulence models have no significant effect on the results.

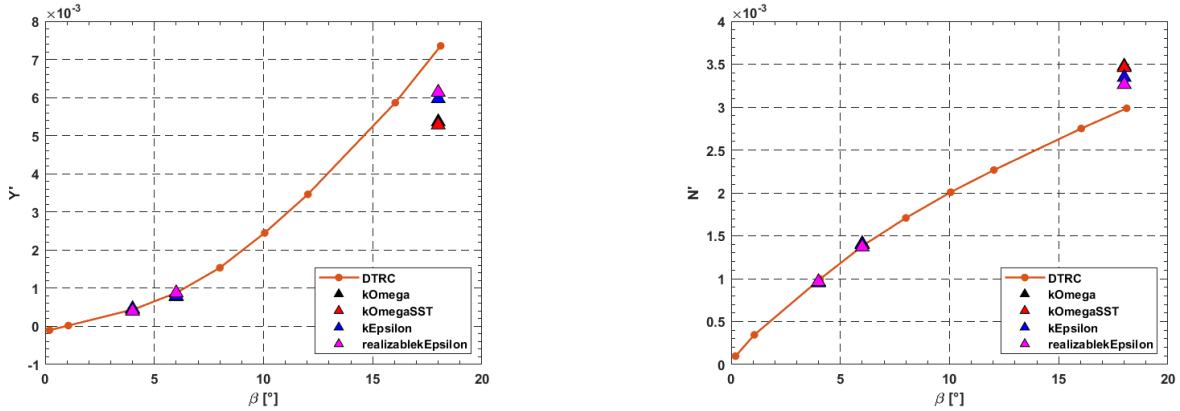

Figure 16. Comparison between the experimental data and the results of the different turbulence models.

5.3 Transition Sensitive Model

Another possible source of discrepancy can be ascribed to the laminar-turbulent transition. Considering that the present test case has been tested at $Re = 1.4 \times 10^7$, means that a significant portion of the body could experience a laminar boundary layer regime. For this region and considering that the Reynolds averaged Navier-stokes (RANS) turbulence models fail to predict these transitional flow features, the RANS transition sensitive model $\gamma - Re_\theta$ (Menter and Langtry, 2012) is used. The kOmegaSSTLM (Shear Stress Transport Linearised Model), an extension of the kOmegaSST (Shear Stress Model) is a transition sensitive turbulence model commonly used and implemented in OpenFOAM (Langtry and Menter, 2009; Menter *et al*., 2006; Langtry, 2006). Tab. 3 shows the comparison between the values of non-dimensional lateral force and yaw moment predicted with the kOmegaSSTLM, the measured data from DTRC, the values from the previous section of realizablekEpsilon (the closest to the experimental data from the previously analysed turbulence models) and those of kOmegaSST. Fig. 17 shows the sectional lateral forces for the two models. As before, its outcomes closer to the experimental data get along with small magnitude of the negative contribution of the sectional forces.

Table 3. Comparison of the lateral force and the yaw moment predicted with kOmegaSST, kOmegaSSTLM and realizablekEpsilon turbulence models and the exerimental data.

	DTRC	***kOmegaSST***	***kOmegaSSTLM***	***realizablekEpsilon***
$Y'_{18^\circ} \times 10^{-3}$	7.355	5.204	6.433	6.139
$N'_{18^\circ} \times 10^{-3}$	2.986	3.482	3.251	3.264

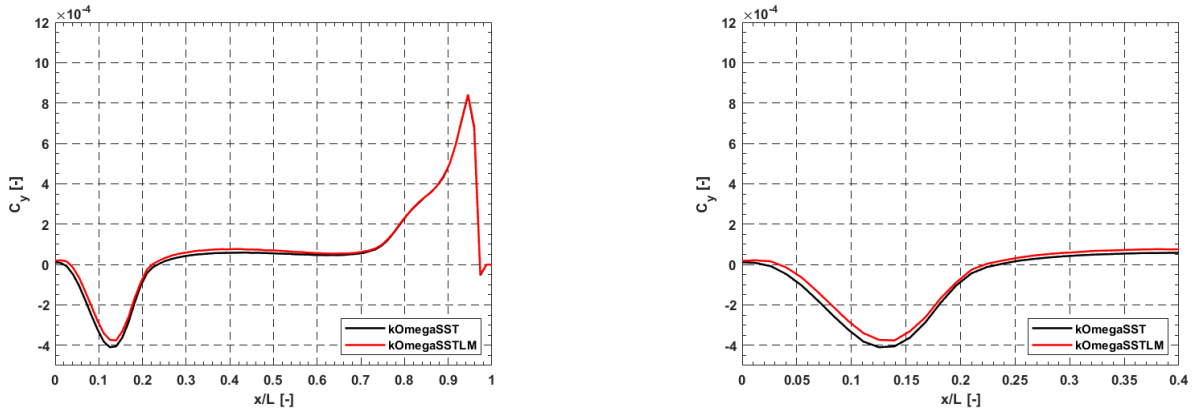

Figure 17. Comparison of the sectional forces calculated with kOmegaSST and kOmegaSSTLM; A closer look to the region of interest where the differences become important.

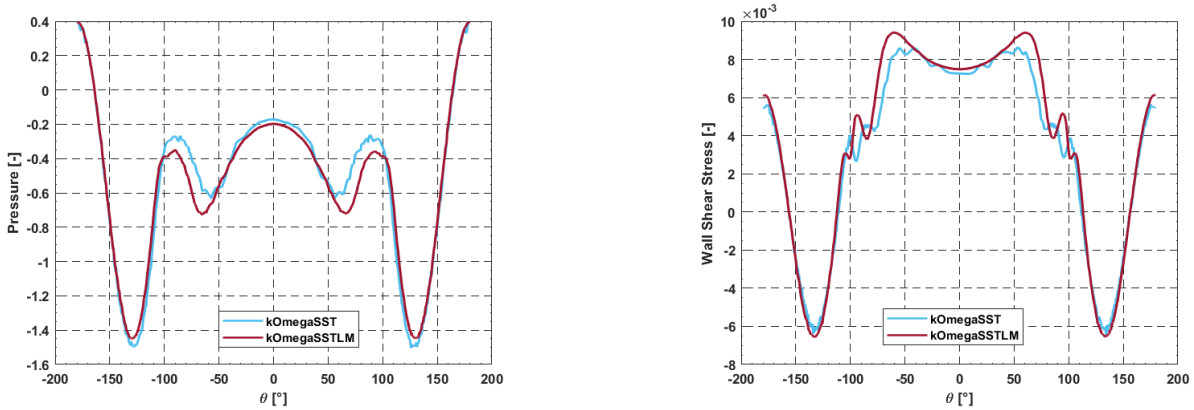

Figure 18. Comparison between the kOmegaSSTLM and kOmegaSST; Pressure distribution (left) and lateral component of wall shear stress values (right) around section B (1.5 m from the aft perperndicular).

The results of this model are clearly somewhat better than those of the realizablekEpsilon, but they still overpredict the yaw moment and underestimate the lateral force. It's interesting to note how the anticipated Y force has larger changes than the predicted N moment in all the different turbulence models used. Fig. 18 shows the distribution of the pressure around section B of the hull (see Fig. 14) and the values of wall shear stress in that region. As analysed before, the influence of the modelling of the vortices in the stern part of the hull is important. In this case the two kOmegaSST models give different outcomes on the pressure field and the shear stress, leading to discrepancies in the sectional lateral forces.

6. CONCLUSIONS

In the author's previous work, an extensive validation of RANS methodologies for the prediction of the hydrodynamic coefficients of the DARPA-SUBOFF model in four different configurations in pure drift and rotation tests was presented. The outcomes showed that for the barehull configuration in high drift angles, two streamwise vortices are generated, having an impact on the non-linearities, and on the prediction of the lateral force and yaw moment. The aim of the current study was to investigate the cause of the discrepancies between the experimental data of the submarine model in barehull configuration and the outcome of the numerical simulations. In the frame of better capturing these vortices, the first attempt was that of analysing the effect of the grid mesh. Even though the results showed that by using more cells the results would converge, the improvement of the predicted values is very small compared to the rapidly growing computational time. The values of the y^+ were also taken into consideration, having simulations with both y^+ between 30 and 50 and smaller than 1. The outcomes are the same between these two cases, demonstrating that the use of the wall-functions is not the primary cause of these errors. The next step focuses on understanding the impact of the different turbulence models. The turbulence models investigated have been kOmega, kOmegaSST, kEpsilon and realizable kEpsilon. As the transitional effects could be important in our case, the RANS transition model $\gamma - Re_\theta$ was also used, more specifically, the results predicted with the kOmegaSSTLM transitional model were compared with the kOmegaSST. Even though the results are slightly better compared to the previous kOmega models (the original model adopted), no differences can be noticed. A more detailed look at the results suggested that the pressure field around the submarine was the same for all models regarding the fore part whereas moving towards the stern these fields are better captured with the kEpsilon models. The lateral contributions of the wall shear stress calculated using the various turbulence models did not differ from one to another. These two observations imply that a better analysis of the pressure field in the stern region of the submarine is needed, thus more accurate turbulence models.

REFERENCES

Broglia R., Posa A., Bettle Marc C., (2020). Analysis of Vortices Shed by a Notional Submarine Model in Steady Drift and Pitch Advancement. *Ocean Engineering*, Volume 218, 108236, ISSN 0029-8018, https://doi.org/10.1016/j.oceaneng.2020.108236.

Carrica P.M., Kim Y., Martin J.E., (2021). Vertical Zigzag Maneuver of a Generic Submarine, *Ocean Engineering*, Volume 219, 108386, ISSN 0029-8018, https://doi.org/10.1016/j.oceaneng.2020.108386.

Chesnakas C.J. and Simpson R.L., (1997). Detailed Investigation of the Three-dimensional Separation about a 6:1 Prolate Spheroid. *American Institute of Aeronautics and Astronautics Journal*, 35(6):990-999.

Dubbioso G., Broglia R., Zaghi S., (2017). CFD Analysis of Turning Abilities of a Submarine Model. *Ocean Engineering*, Volume 129, Pages 459-479, ISSN 0029-8018, https://doi.org/10.1016/j.oceaneng.2016.10.046.

Efremov, D.V., and Milanov E.M., (2019). Hydrodynamics of DARPA SUBOFF Submarine at Shallowly Immersion Conditions. *TransNav: International Journal on Marine Navigation and Safety of Sea Transportation*.

Franceschi A., Piaggio B., Tonelli R., Villa D., Viviani M., (2021). Assessment of the Manoeuvrability Characteristics of a Twin Shaft Naval Vessel Using an Open-source CFD Code. *Journal of Marine Science and Engineering*, 9 (6), art. no. 665. doi: 10.3390/jmse9060665.

Fureby C., Anderson B., D. Clarke, L. Erm, Henbest S., Giacobello M., Jones D., Nguyen M., Johansson M., Jones M., Kumar C., Lee S.K., Manovski P., Norrison D., Petterson K., Seil G., Woodyatt B., Zhu S., (2016). Experimental and Numerical Study of a Generic Conventional Submarine at 10° Yaw. *Ocean Engineering*, Volume 116, Pages 1-20, ISSN 0029-8018, https://doi.org/10.1016/j.oceaneng.2016.01.001.

Haipeng Guo, Guangnian Li, Lin Du, (2023). Investigation on the Flow around a Submarine under the Rudder Deflection Condition by using URANS and DDES Methods. *Applied Ocean Research*, Volume 131, 103448, ISSN 0141-1187, https://doi.org/10.1016/j.apor.2022.103448.

Khan, Md Kareem, et al. (2022). Surface Pressure Measurements on a Generic Submarine Hull Form at High Angles of Incidence. *Journal of Marine Science and Technology*, 27.1: 677-694.

Kotapati-Apparao R.B., Squires K. D., and Forsythe J. R., (2003). Prediction of a Prolate Spheroid Undergoing a Pitchup Maneuver. *AIAA Paper*, 2003-02-69:1-11.

Kumar C., Manovski P. and Giacobello M., (2012). Particle Image Velocimetry Measurements on a Generic Submarine Hull Form. *The 18th Australasian Fluid Mechanics Conference*.

Langtry, R. B. and Menter, F. R., (2009). Correlation-Based Transition Modeling for Unstructured Parallelized Computational Fluid Dynamics Codes. *AIAA Journal***,** Vol. 47, No. 12, pp. 2894-2906, https://doi.org/10.2514/1.42362.

Liu Y.; Zhou, Zhiteng; Zhu, Lixing; Wang, Shizhao, (2021). Numerical Investigation of Flows around an Axisymmetric Body of Revolution by Using Reynolds-Stress Model Based Hybrid Reynolds-Averaged Navier–Stokes/Large Eddy Simulation. *Physics of Fluids*, 33, ISSN 1070-6631, https://doi.org/10.1063/5.0058016.

Lungu A., (2019). DES-Based Computation of the Flow around the DARPA SUBOFF, *IOP Conf.Ser.*: Mater Sxi.Eng.591, 012053, https://doi.org/10.1088/1757-899X/591/1/012053.

Manshadi, Mojtaba Dehghan, Kazem Hejranfar, and Amir Hamzeh Farajollahi, (2017). Effect of Vortex Generators on Hydrodynamic Behavior of an Underwater Axisymmetric Hull at High Angles of Attack. *Journal of Visualization* 20: 559-579.

Menter, F.R., (1994). Two-Equation Eddy-Viscosity Turbulence Models for Engineering Applications. *AIAA J.*, 32, 1598–1605. https://doi.org/10.2514/3.12149.

Menter F. R. and Laungtry B. R., (2012). Transition Modelling for Turbomachinery Flows. Low Reynolds Number Aerodynamics and Transition. *InTech*. DOI: 10.5772/38675.

Morse, N., & Mahesh, K., (2021). Large-Eddy Simulation and Streamline Coordinate Analysis of Flow over an Axisymmetric Hull. *Journal of Fluid Mechanics*, 926, A18, https://doi.org/10.1017/jfm.2021.714.

Piaggio B., Villa D., Viviani M., (2020) Numerical Analysis of Escort Tug Manoeuvrability Characteristics. *Applied Ocean Research*, 97, art. no. 102075. doi: 10.1016/j.apor.2020.102075.

Pope Stephen B., (2000). *Turbulent Flows*, Cornell University, New York, USA.

Posa, A., & Balaras, E., (2016) A numerical investigation of the wake of an axisymmetric body with appendages. Journal of Fluid Mechanics, 792, 470-498, https://doi.org/10.1017/jfm.2016.47.

Rocca A., Cianferra M., Broglia R., Armenio V., (2022). Computational Hydroacoustic Analysis of the BB2 Submarine using the Advective Ffowcs Williams and Hawkings Equation with Wall-Modeled LES. *Applied Ocean Research*, Volume 129, 103360, ISSN 0141-1187, https://doi.org/10.1016/j.apor.2022.103360.

Roddy R.F., (1990). Investigation of the Stability and Control Characteristics of Several Configurations of the DARPA SUBOFF Model (DTRC Model 5470) from Captive-model Experiments. David Taylor Research Center, SHD 1298-08, Maryland, USA.

Strelets M., (2001). Detached Eddy Simulation of Massively Separated Flows. *39th Aerospace Sciences Meeting and Exhibit*, Reno, 8-11 January 2001, 879. https://doi.org/10.2514/6.2001-879.

Subrahmanya M.B., Rajani B.N., (2019). Numerical Investigation of the Flow Past 6:1 Prolate Spheroid. *21st Annual CFD Symposium*, Bangalore.

Van Doormall, J.P. and Raithby, G.D. (1984) Enhancements of the Simple Method for Predicting Incompressible Fluid Flows. *Numerical Heat Transfer*, 7, 147-163.

Wackers J., Deng G., Guilmineau E., Leroyer A., Queutey P., Visonneau M., (2015). *What is happening around the KVLCC2*, NuTTS, Cortona, Italy.

Wang L., J. Ezequiel Martin, Mario Felli, Pablo M. Carrica (2020). Experiments and CFD for the Propeller Wake of a Generic Submarine Operating near the Surface. *Ocean Engineering*, Volume 206, 107304, ISSN 0029-8018, https://doi.org/10.1016/j.oceaneng.2020.107304.

Wang L., Martin J.E., Carrica P.M., Felli M., Falchi M., (2019). Experiments and CFD for DARPA SUBOFF Appended with Propeller E1658 Operating near the Surface, *6th International Symposium on Marine Propulsors.*

Zhang, Z., Guo, L., Wei, P. et al., (2020). Numerical Simulation of Submarine Surfacing Motion in Regular Waves. *Iran J Sci Technol Trans Mech Eng* ,44, 359–372. https://doi.org/10.1007/s40997-018-0259-5

Zheku V.V., Villa D., Piaggio B., Gaggero S., Viviani M. (2023 under review) Assesment of the Numerical Captive Model Tests for the Underwater Vehicles: the DARPA SUB-OFF test case. *Ocean Engineering.*